ORIGINAL SCIENTIFIC PAPER

CROATICA CHEMICA ACTA

Croat. Chem. Acta **2016**, *89*(1), 117–124
Published online: June 7, 2016
DOI: 10.5562/cca2797

HKD 1926

Study of Dronino Iron Meteorite Weathering in Clay Sand Using Mössbauer Spectroscopy

Grigoriy A. Yakovlev,[1] Andrei V. Chukin,[2] Victor I. Grokhovsky,[1] Vladimir A. Semionkin,[3] Michael I. Oshtrakh[1,3,*]

[1] Department of Physical Techniques and Devices for Quality Control, Institute of Physics and Technology, Ural Federal University, Ekaterinburg 620002, Russian Federation

[2] Department of Theoretical Physics and Applied Mathematics, Institute of Physics and Technology, Ural Federal University, Ekaterinburg 620002, Russian Federation

[3] Department of Experimental Physics, Institute of Physics and Technology, Ural Federal University, Ekaterinburg 620002, Russian Federation

* Corresponding author's e-mail address: oshtrakh@gmail.com

RECEIVED: December 1, 2015 * REVISED: April 29, 2016 * ACCEPTED: April 29, 2016

THIS PAPER IS DEDICATED TO DR. SVETOZAR MUSIĆ ON THE OCCASION OF HIS 70TH BIRTHDAY

Abstract: Weathering products of two fragments of Dronino iron ungrouped meteorite found in the wet and drier clay sand were studied using X-ray diffraction and Mössbauer spectroscopy with a high velocity resolution. The products of metal oxidation in the internal and external surface layers were different for both fragments. The weathering products in fragment found in the wet clay sand contain magnetite (Fe_3O_4), maghemite (γ-Fe_2O_3), goethite (α-FeOOH) and probably ferrihydrite ($5Fe_2O_3 \cdot 9H_2O$) while those in fragment found in drier clay sand contained ferric hydrous oxides (FeOOH) and siderite ($FeCO_3$) mainly. Concretions found near the first fragment contain ferric hydrous oxides (FeOOH) mainly.

Keywords: Dronino iron ungrouped meteorite, weathering, ferric oxides and hydrous oxides, siderite, Mössbauer spectroscopy.

INTRODUCTION

DRONINO meteorite shower was found in July 2000 near the Dronino village, Ryazan District, Russian Federation. This meteorite was classified as iron ungrouped meteorite (see Meteoritical Bulletin № 88, 2004). Terrestrial age of this meteorite can be evaluated as more than 1000 years. The first meteorite fragments demonstrated heavily weathering with a rust-covered surface of several centimeters thickness. The Meteoritical Expedition of the Ural Federal University found several fragments of Dronino meteorite in different places of the fall in the clay sand at a depth of ~0.5 – ~2.0 m. A photo of the place where one fragment was found in water-bearing soil is shown in Figure 1a. All surrounded clay sand was colored in reddish-brown due to the rust diffusion mass transfer. Several concretions formed in this place were also found. Some of these samples were studied using Mössbauer spectroscopy earlier.[1,2] However, these first measurements were carried out using the low velocity resolution in the Mössbauer spectra (smaller discretization of the velocity scale in the spectra). Further, with the development of technique application, the high velocity resolution Mössbauer spectroscopy (high discretization of both the velocity reference signal and the velocity scale in the spectra) demonstrated significant advances in the study of the complicated spectra of various meteorites in order to extract more detailed information.[3–7] Therefore, in the present work we discuss the results of re-examination of the first samples of Dronino oxidation products in comparison with new samples studied with the high velocity resolution Mössbauer spectroscopy.

EXPERIMENTAL

Two fragments of Dronino iron ungrouped meteorite found in two different places of clay sand were chosen for the study of metal surface oxidation and denoted as № 1 and № 2. Fragment № 1 was found in the water-bearing soil (the wet clay sand) shown in Figure 1a while fragment № 2

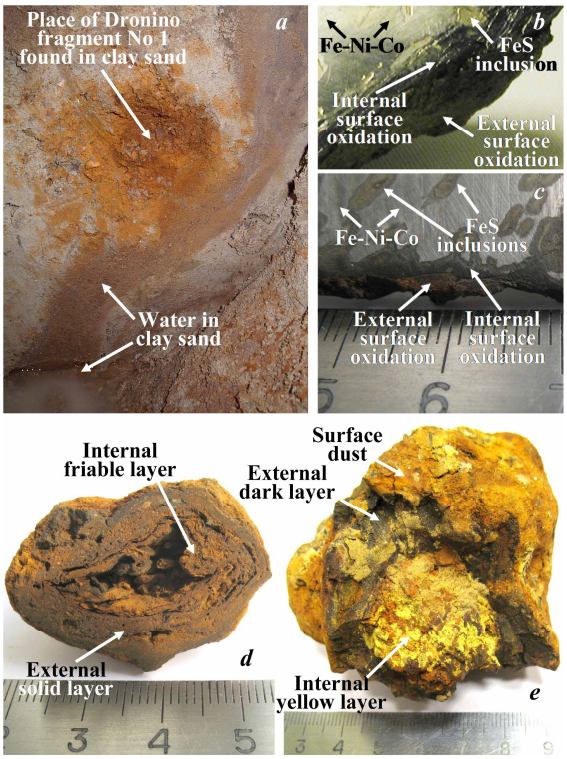

Figure 1. The place of the clay sand where Dronino iron ungrouped fragment № 1 was found (a), the places where samples were taken from the internal and external surface oxidation layers in Dronino fragments № 1 (b) and № 2 (c), and from the internal and external layers in concretions № 3 (d) and № 4 (e) and surface dust on concretion № 4.

was found in the drier clay sand. The rust layer was removed and fragments were cut (their slices are shown in Figure 1b,c). Oxidized surface can be conventionally divided into two layers denoted as internal (which are denoted as № 1a and № 2a for fragments № 1 and № 2, respectively) and external (which are denoted as № 1b and № 2b for fragments № 1 and № 2, respectively) surface oxidation layers which can be distinguished in their color for fragment № 2 (see Figure 1c). These layers were removed from both fragments and grounded. Two samples of concretions, found in the wet clay sand, with different size and color (small № 3 and big № 4) shown in Figure 1d,e were chosen for this study also. Two parts of each concretion were taken for analysis: the internal friable and the external solid layers from № 3 (which are denoted as № 3a and № 3b, respectively) and the yellow-colored internal and the dark-colored external layers from № 4 (which are denoted as № 4a and № 4b, respectively). These samples were also grounded. Additionally, the surface yellow dust (which is denoted as № 4c) was collected from concretion № 4. These powdered samples were used for X-ray diffraction (XRD) study and then were glued on the iron free aluminum foil with a diameter of ~20 mm. The weight of each sample was in the range 30–60 mg that provided the thin absorbers for Mössbauer measurements.

XRD study was carried out using PANalytical X'pert PRO diffractometer (The Netherlands) with Cu Kα radiation and position-sensitive X'Celerator detector with Ni filter. Measurements were done in 2Θ ranges between 10 ° and 100 ° with a step of 0.026 ° and 200 s per step.

Mössbauer spectra were measured using an automated precision Mössbauer spectrometric system built on the base of the SM-2201 spectrometer with a saw-tooth shape velocity reference signal formed by the digital-analogue converter using quantification of 2^{12} (discretization with 4096 steps). This discretization of the velocity reference signal (velocity resolution) produces smaller step in Doppler modulation of resonant γ-rays energy providing much better adjusting to resonance and significantly increases the quality of spectra measurements. This also increases the analytical possibilities of Mössbauer spectroscopy with extracting more reliable spectral components in the complex spectra due to larger number of spectral points and better measurement of the absorption line shape features. Characteristics of this system were described elsewhere.[8–10] The 1.8×10^9 Bq ^{57}Co(Rh) source (Ritverc GmbH, St. Petersburg) was used at room temperature. The Mössbauer spectra were measured in transmission geometry with moving absorber in the cryostat at 295 K and recorded in 4096 channels. For their analysis the spectra were converted into 2048 channels to increase signal-to-noise ratio for the smallest spectral components. Statistics in the Mössbauer spectra was in the range ~1.0×10^6 and ~2.6×10^6 counts per channel with signal-to-noise ratio in the range 43–104. Each spectrum was measured during 3–7 days. Mössbauer spectra were fitted by the least squares procedure with a Lorentzian line shape using UNIVEM-MS program. The line shape of the Mössbauer spectrum of the standard absorber of α-Fe with a thickness of 7 μm was pure Lorentzian with outer lines width of 0.236±0.008 mm s^{-1}. Velocity resolution (velocity per one channel) was ~0.010–~0.014 mm s^{-1} per channel for the 2048 channels Mössbauer spectra. The spectral parameters isomer shift, δ, quadrupole splitting (quadrupole shift for magnetically split components), ΔE_Q, magnetic hyperfine field, H_{eff}, line width, Γ, relative subspectrum area, A, and statistical quality of the fit, χ^2, were determined. Criteria of the best fit were differential spectrum, χ^2, and physical meaning of parameters. An instrumental (systematic) error for each spectrum point was ±0.5 channel (the velocity scale), the instrumental (systematic) error for the hyperfine parameters was ±1 channel. The relative instrumental error for A did not exceed 10 %. If an error

calculated during the fit (fitting error) for these parameters exceeded the instrumental (systematic) error we used the largest error. Values of δ are given relative to α-Fe at 295 K.

RESULTS AND DISCUSSION

XRD patterns of the studied samples are shown in Figure 2. The internal oxidation products in fragment № 1 contain mainly magnetite/maghemite Fe_3O_4/γ-Fe_2O_3 (it is not too easy to distinguish both oxides using these XRD measurements) and ferric hydrous oxides (FeOOH) while the external oxidation products demonstrate the presence of ferric hydrous oxides mainly (we consider iron-containing phases only). In contrast, the internal and external surface oxidation products in fragment № 2 contain a large amount of siderite ($FeCO_3$) and ferric hydrous oxides. Both layers in concretion № 3 and the yellow internal layer in concretion № 4 contain ferric hydrous oxides only while dark external layer in concretion № 4 contains siderite additionally. An analysis of ferric hydrous oxides patterns showed that their main part was in the form of goethite (α-FeOOH) while some amount of ferrihydrite ($5Fe_2O_3 \cdot 9H_2O$) and other forms of ferric hydrous oxides could be also considered.

Mössbauer spectra of the internal and external surface oxidation layers in fragments № 1 and № 2 are shown in Figure 3. The spectra of the internal and external weathering products were different for each fragment. Moreover, the spectra of both internal and external oxidation products appeared to be different for fragments № 1 and № 2, respectively. The results of the best fits of these spectra are shown in Figure 3 and parameters are presented in Table 1. An analysis of components 1–5 in the Mössbauer spectrum of the internal oxidation products in Dronino fragment № 1 (Figure 3a) on the basis of previously published data on iron oxides and hydroxides (see, for instance[11–16]) permitted us to distinguish components 1, 3 and 2, 4, 5 and assigned these components to maghemite and magnetite, respectively. Component 1 was related to the ^{57}Fe in the octahedral sites [B] while component 3 was related to the ^{57}Fe in the tetrahedral sites (A) in γ-Fe_2O_3. In contrast, component 2 was related to the (A) sites in Fe_3O_4 while two components 4 and 5 were related to the ^{57}Fe in the [B] sites in Fe_3O_4. Two components related to the [B] sites may be related to the presence of ~9.3 at.% Ni in the matrix Fe-Ni-Co alloy in Dronino iron meteorite which can substitute Fe^{3+} in the [B] positions forming Ni^{2+}-containing magnetite during the weathering similar to $NiFe_2O_4$ inverse spinel in which nickel cations can occupy [B] sites only and their different numbers in the iron local environment may be a reason of different magnetic hyperfine fields on the ^{57}Fe nuclei (see Refs. [17,18]). Other magnetic sextets 6–8 were associated with goethite small particles with different

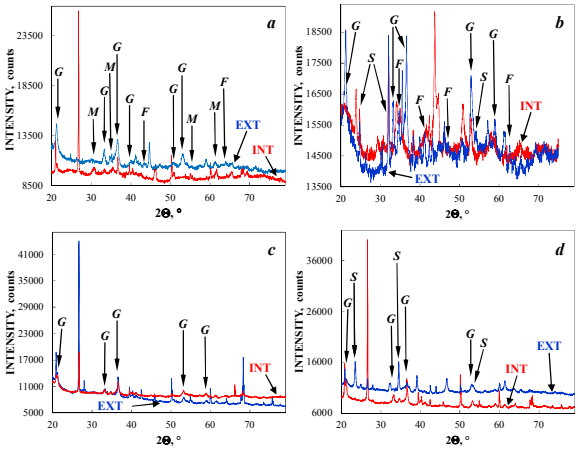

Figure 2. X-ray diffraction patterns of the internal (INT) and external (EXT) surface oxidation products in Dronino fragments № 1 (a) and № 2 (b) and the internal (INT) and external (EXT) surface layers in concretions № 3 (c) and № 4 (d). Indicated selected reflexes are magnetite/maghemite, PDF-2: 01-089-0951 (M), goethite, PDF-2: 00-029-0713 (G), ferrihydrite, PDF-2: 00-029-0712 (F) and siderite, PDF-2: 01-083-1764 (S).

size and smaller values of H_{eff} than that for bulk α-FeOOH (the Néel temperature is 400 K[16]). Similar decrease of the values of H_{eff} with the decreasing of goethite nanoparticles size was observed in Ref. [19]. Three paramagnetic quadrupole doublets demonstrate hyperfine parameters indicating the presence of ferric compounds. These components can be assigned to paramagnetic goethite nanoparticles and/or ferrihydrite small particles (the latter Néel temperature is below 100 K). Therefore, these components were related to ferric hydrous oxides FeOOH (nanosized goethite and/or ferrihydrite). In the Mössbauer spectrum of the external oxidation products in Dronino fragment № 1 (Figure 3b) we revealed four magnetic sextets 1–4 which can be related to α-FeOOH small particles with different size and variations in the values of H_{eff} (smaller value of δ for component 2 rises a question concerning the possibility to relate this parameter to goethite). Three paramagnetic components had hyperfine parameters corresponding to ferric compounds. However, Mössbauer parameters for quadrupole doublets 5 and 6 could be related to FeOOH (nanosized goethite and/or ferrihydrite) while component 7 had larger value of δ than that for ferric hydrous oxides.

Quite different results were obtained for both internal and external oxidation products in Dronino fragment № 2. The Mössbauer spectrum of the internal oxidation products in fragment № 2 (Figure 3c) demonstrated two weak and broad magnetic sextets 1 and 2. Their hyperfine parameters can be related to the presence of Fe-Ni-Co alloy matrix (due to the sample preparation) and goethite particles,

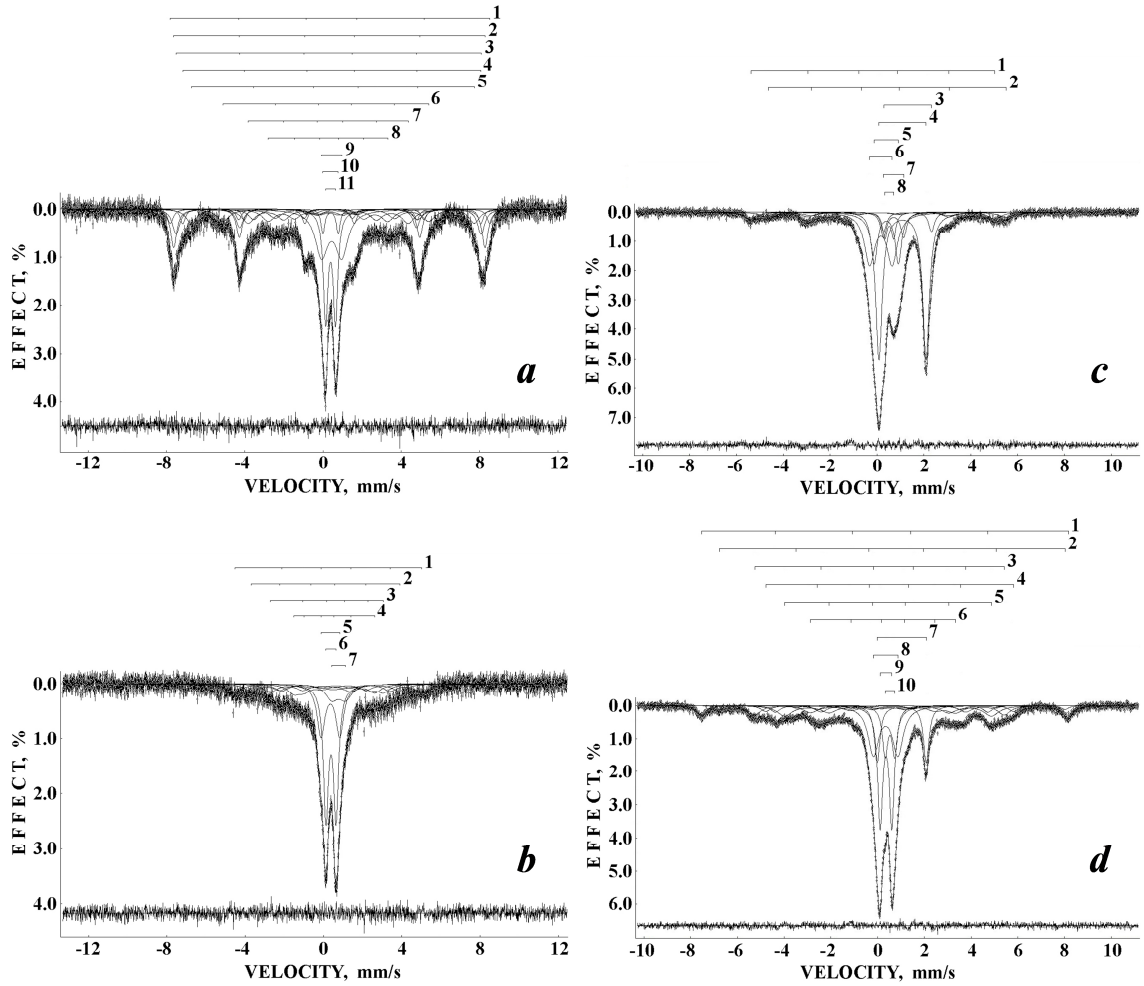

Figure 3. Mössbauer spectra of the internal (a) and external (b) surface oxidation products in Dronino fragment № 1 and the internal (c) and external (d) surface oxidation products in Dronino fragment № 2. Indicated components are the results of the best fits (parameters of components see in Table 1). Differential spectra are shown below. T = 295 K.

respectively. Two quadrupole doublets 3 and 4 had hyperfine parameters characterized the presence of ferrous compounds while the other quadrupole doublets 5–8 demonstrated the presence of ferric compounds. The values of ΔE_Q and δ for components 3 and 4 were similar to siderite which parameters varied in the ranges of ΔE_Q ~1.6–2.0 mm s^{-1} and δ ~1.2–1.3 mm s^{-1} (see Refs. [20–23]). Basing on XRD data about the presence of $FeCO_3$ in the weathering products of Dronino fragment № 2 we assigned both components 3 and 4 to siderite with some possible small variations in the iron local microenvironment. Paramagnetic quadrupole doublets 5, 6 and 8 were related to FeOOH (nanosized goethite and/or ferrihydrite) with open question concerning smaller value of δ for component 6. Quadrupole doublet 7 had hyperfine parameters characterized ferric compound. The Mössbauer spectrum of the external oxidation products in Dronino fragment № 2 (Figure 3d) demonstrated more spectral components. Two magnetic sextets 1 and 2 were related to the ^{57}Fe in the (A) and [B] sites in magnetite while the other magnetic sextets 3–6 were assigned to goethite small particles with different size and variations in the values of H_{eff}. Paramagnetic quadrupole doublet 7 with Mössbauer parameters indicating the ferrous compound was related to $FeCO_3$ like similar components 3 and 4 in the Mössbauer spectrum of the internal weathered products (Figure 3c). Paramagnetic components 8 and 9 were assigned to FeOOH (nanosized goethite and/or ferrihydrite) while component 10 was related to ferric compound.

The Mössbauer spectra of concretions' samples are shown in Figure 4. These spectra demonstrated the presence of magnetic and paramagnetic (superparamagnetic)

Table 1. Mössbauer parameters of the surface oxidation products from Dronino iron meteorite fragments № 1 and № 2

Sample	Γ / mm s^{-1}	δ / mm s^{-1}	ΔE_Q / mm s^{-1}	H_{eff} / kOe	A / %	Component[a]
№ 1a, internal surface oxidation products	0.363 ± 0.073	0.397 ± 0.015	–0.065 ± 0.024	507.1 ± 2.1	5	γ-Fe_2O_3 [B] (1)
	0.376 ± 0.036	0.332 ± 0.013	–0.009 ± 0.013	494.0 ± 0.9	13	Fe_3O_4 (A) (2)
	0.449 ± 0.047	0.277 ± 0.017	0.029 ± 0.027	483.9 ± 1.9	10	γ-Fe_2O_3 (A) (3)
	0.314 ± 0.081	0.425 ± 0.023	0.056 ± 0.029	472.8 ± 1.8	4	Fe_3O_4 [B1] (4)
	0.664 ± 0.068	0.578 ± 0.018	–0.146 ± 0.035	449.0 ± 1.9	8	Fe_3O_4 [B2] (5)
	0.776 ± 0.070	0.380 ± 0.021	–0.456 ± 0.040	326.4 ± 1.5	9	α-FeOOH (6)
	0.776 ± 0.026	0.316 ± 0.019	–0.095 ± 0.033	253.9 ± 1.7	10	α-FeOOH (7)
	0.776 ± 0.026	0.286 ± 0.025	–0.057 ± 0.040	189.6 ± 1.5	8	α-FeOOH (8)
	0.776 ± 0.026	0.444 ± 0.013	1.033 ± 0.019	–	16	FeOOH (9)
	0.233 ± 0.026	0.389 ± 0.013	0.782 ± 0.014	–	3	FeOOH (10)
	0.284 ± 0.026	0.390 ± 0.013	0.503 ± 0.013	–	14	FeOOH (11)
№ 1b, external surface oxidation products	0.776 ± 0.026	0.425 ± 0.040	–0.344 ± 0.071	297.3 ± 1.9	11	α-FeOOH (1)
	0.776 ± 0.026	0.104 ± 0.048	–0.036 ± 0.091	236.8 ± 2.7	10	? α-FeOOH (2)
	0.776 ± 0.154	0.349 ± 0.040	–0.303 ± 0.076	177.8 ± 2.8	10	α-FeOOH (3)
	0.776 ± 0.026	0.442 ± 0.051	0.270 ± 0.082	126.5 ± 3.7	9	α-FeOOH (4)
	0.423 ± 0.034	0.322 ± 0.013	0.926 ± 0.027	–	14	FeOOH (5)
	0.300 ± 0.026	0.379 ± 0.013	0.514 ± 0.013	–	28	FeOOH (6)
	0.767 ± 0.106	0.604 ± 0.032	0.750 ± 0.028	–	18	Fe^{3+} compound (7)
№ 2a, internal surface oxidation products	0.653 ± 0.055	–0.065 ± 0.024	–0.235 ± 0.047	322.7 ± 0.8	7	? Fe-Ni-Co (1)
	0.776 ± 0.077	0.287 ± 0.039	0.297 ± 0.071	315.1 ± 1.2	6	α-FeOOH (2)
	0.293 ± 0.025	1.306 ± 0.011	2.042 ± 0.297	–	4	$FeCO_3$ 1 (3)
	0.342 ± 0.022	1.087 ± 0.011	2.011 ± 0.011	–	38	$FeCO_3$ 2 (4)
	0.326 ± 0.022	0.395 ± 0.011	1.034 ± 0.011	–	13	FeOOH (5)
	0.541 ± 0.022	0.165 ± 0.011	0.961 ± 0.011	–	21	? FeOOH (6)
	0.299 ± 0.022	0.709 ± 0.011	0.858 ± 0.014	–	6	Fe^{3+} compound (7)
	0.233 ± 0.022	0.521 ± 0.011	0.374 ± 0.011	–	5	FeOOH (8)
№ 2b, external surface oxidation products	0.474 ± 0.028	0.245 ± 0.011	0.154 ± 0.021	487.6 ± 0.6	7	Fe_3O_4 (A) (1)
	0.399 ± 0.063	0.708 ± 0.021	–0.167 ± 0.042	459.3 ± 1.3	2	Fe_3O_4 [B] (2)
	0.628 ± 0.050	0.375 ± 0.014	–0.592 ± 0.038	331.5 ± 0.8	8	α-FeOOH (3)
	0.495 ± 0.077	0.500 ± 0.022	0.030 ± 0.043	329.3 ± 1.2	4	α-FeOOH (4)
	0.776 ± 0.044	0.462 ± 0.012	–0.040 ± 0.022	274.8 ± 1.2	11	α-FeOOH (5)
	0.776 ± 0.067	0.444 ± 0.021	–0.427 ± 0.033	192.7 ± 1.2	7	α-FeOOH (6)
	0.286 ± 0.022	1.031 ± 0.011	2.100 ± 0.011	–	11	$FeCO_3$ (7)
	0.549 ± 0.022	0.343 ± 0.011	1.044 ± 0.011	–	18	FeOOH (8)
	0.260 ± 0.022	0.358 ± 0.011	0.496 ± 0.011	–	21	FeOOH (9)
	0.274 ± 0.022	0.527 ± 0.011	0.411 ± 0.011	–	9	Fe^{3+} compound (10)

[a] Components correspond to spectral components indicated in Figure 3.

components for the internal friable and external solid layers in concretion № 3 and for the internal yellow layer in concretion № 4. The spectra of the external dark layer and surface dust in concretion № 4 consisted of paramagnetic (superparamagnetic) components only. The results of the best fits of these spectra are shown in Figure 4 and parameters are presented in Table 2. All magnetic sextets in these spectra demonstrated hyperfine parameters which can be related to α-FeOOH small particles with different size and variations in the values of H_{eff}. All paramagnetic quadrupole doublets demonstrating hyperfine parameters typical for ferric compounds (except component 1 in Figure 4d with parameters related to ferrous compound) were assigned to FeOOH (nanosized goethite and/or ferrihydrite). Ferrous compound observed in the Mössbauer spectrum of the external dark layer in concretion № 4 had the values of ΔE_Q and δ similar to siderite.

The results of the study of Dronino iron meteorite weathering products using XRD and Mössbauer spectroscopy demonstrated the difference in the surface oxidation of fragment № 1 found in the wet clay sand and fragment № 2 found in the drier clay sand. The internal oxidation products in fragment № 1 consisted of maghemite, magnetite and ferric hydrous oxides, mainly goethite, while the external oxidation products contained ferric hydrous oxides and unidentified ferric compound. It is possible that oxidation of the Fe-Ni-Co alloy in Dronino fragment led to formation of magnetite with its further oxidation to maghemite. Then maghemite interaction with water led to formation of ferric hydrous oxides. This process moves inside the metal while the external surface layer contains ferric hydrous oxides only. These ferric hydrous oxides are in the form of small particles and/or nanoparticles demonstrating superparamagnetic behavior at room temperature. These

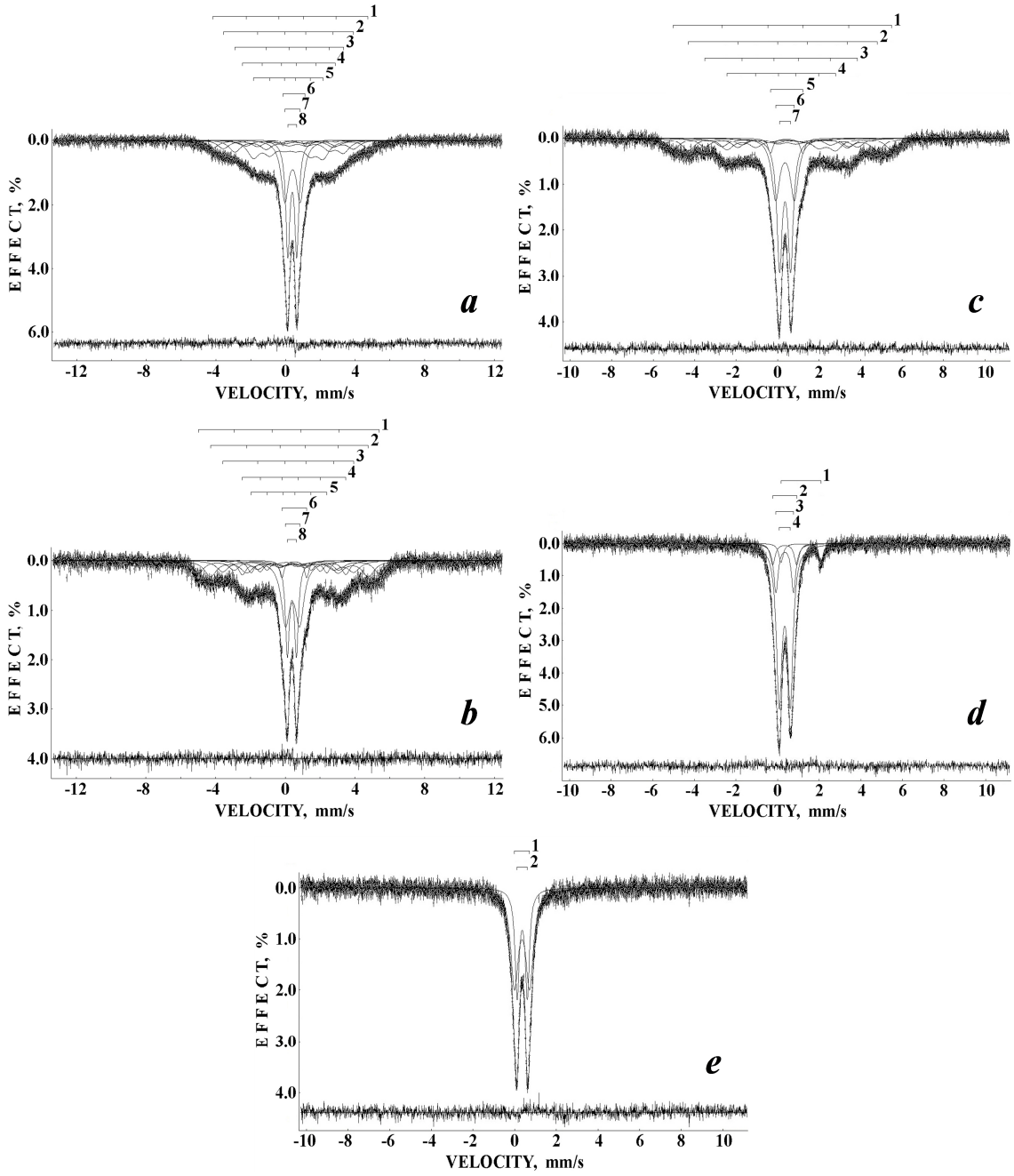

Figure 4. Mössbauer spectra of the internal (a) and external (b) layers from concretion № 3 and the internal (c) and external (d) layers and surface dust (e) from concretion № 4. Indicated components are the results of the best fits (parameters of components see in Table 2). Differential spectra are shown below. *T* = 295 K.

particles as well as individual FeOOH molecules can diffuse or be transferred into the clay sand with changing its color and further formation of concretions. These concretions consist of ferric hydrous oxides with different sizes of FeOOH particles/nanoparticles showed different superparamagnetic behavior of the internal and external layers at room temperature. The oxidation process in Dronino fragment № 2 was quite different. The internal surface oxidation products contain ferric hydrous oxides, siderite and unidentified ferric compound while the external surface weathering products consist of small amount of magnetite, ferric hydrous oxides, siderite and unidentified ferric compound. It should be noted that siderite formation in clay may be a result of bioreduction of goethite by

Table 2. Mössbauer parameters of concretions matter found in Dronino fragments surrounded clay sand

Sample	Γ / mm s^{-1}	δ / mm s^{-1}	ΔE_Q / mm s^{-1}	H_{eff} / kOe	A / %	Component[a]
№ 3a, internal friable layer	0.834 ± 0.078	0.302 ± 0.030	–0.044 ± 0.055	277.1 ± 1.5	10	α-FeOOH (1)
	0.833 ± 0.061	0.366 ± 0.027	–0.392 ± 0.053	232.4 ± 2.1	10	α-FeOOH (2)
	0.834 ± 0.141	0.454 ± 0.018	–0.485 ± 0.031	193.7 ± 2.4	14	α-FeOOH (3)
	0.488 ± 0.310	0.199 ± 0.055	0.004 ± 0.109	165.8 ± 5.2	2	? α-FeOOH (4)
	0.833 ± 0.061	0.209 ± 0.017	–0.103 ± 0.035	124.4 ± 1.4	20	? α-FeOOH (5)
	0.233 ± 0.092	0.485 ± 0.018	1.267 ± 0.035	–	1	FeOOH (6)
	0.517 ± 0.026	0.408 ± 0.013	0.879 ± 0.015	–	21	FeOOH (7)
	0.283 ± 0.028	0.391 ± 0.026	0.511 ± 0.013	–	22	FeOOH (8)
№ 3b, external solid layer	0.748 ± 0.067	0.137 ± 0.029	0.132 ± 0.056	321.7 ± 1.6	13	? α-FeOOH (1)
	0.834 ± 0.026	0.327 ± 0.019	–0.173 ± 0.027	281.1 ± 1.7	17	α-FeOOH (2)
	0.834 ± 0.026	0.382 ± 0.029	–0.425 ± 0.052	233.7 ± 2.3	12	α-FeOOH (3)
	0.559 ± 0.066	0.395 ± 0.018	0.223 ± 0.034	184.6 ± 1.3	10	α-FeOOH (4)
	0.470 ± 0.055	0.213 ± 0.019	–0.007 ± 0.027	135.2 ± 1.2	7	? α-FeOOH (5)
	0.294 ± 0.048	0.521 ± 0.013	1.425 ± 0.022	–	3	FeOOH (6)
	0.600 ± 0.030	0.422 ± 0.013	0.812 ± 0.024	–	22	FeOOH (7)
	0.271 ± 0.026	0.383 ± 0.013	0.517 ± 0.013	–	16	FeOOH (8)
№ 4a, internal yellow layer	0.776 ± 0.064	0.302 ± 0.018	–0.147 ± 0.033	327.2 ± 1.4	13	α-FeOOH (1)
	0.776 ± 0.079	0.483 ± 0.016	–0.472 ± 0.031	282.6 ± 1.2	14	α-FeOOH (2)
	0.776 ± 0.086	0.289 ± 0.023	–0.245 ± 0.040	228.7 ± 1.6	10	α-FeOOH (3)
	0.776 ± 0.065	0.317 ± 0.016	–0.286 ± 0.028	162.9 ± 1.3	13	α-FeOOH (4)
	0.301 ± 0.034	0.432 ± 0.010	1.526 ± 0.017	–	3	FeOOH (5)
	0.470 ± 0.020	0.356 ± 0.010	0.902 ± 0.010	–	19	FeOOH (6)
	0.309 ± 0.020	0.359 ± 0.010	0.532 ± 0.010	–	27	FeOOH (7)
№ 4b, external dark layer	0.250 ± 0.022	1.129 ± 0.011	1.931 ± 0.012	–	6	FeCO3 (1)
	0.292 ± 0.022	0.341 ± 0.011	1.097 ± 0.011	–	12	FeOOH (2)
	0.254 ± 0.022	0.345 ± 0.011	0.800 ± 0.011	–	17	FeOOH (3)
	0.318 ± 0.022	0.343 ± 0.011	0.519 ± 0.011	–	64	FeOOH (4)
№ 4c, surface dust	0.445 ± 0.022	0.355 ± 0.011	0.723 ± 0.034	–	62	FeOOH (1)
	0.244 ± 0.022	0.363 ± 0.011	0.488 ± 0.011	–	38	FeOOH (2)

[a] Components correspond to spectral components indicated in Figure 4.

bacteria.[24] Therefore, bacteria can live inside the internal oxidation layer in the drier clay sand with conversion of goethite into siderite moving inside the metal matrix with the oxidation process. Observation of small amount of siderite in the external dark layer in concretion № 4 may also be a result of goethite bioreduction, however, bacteria in this case might convert goethite into siderite at the early stage of concretion formation with further stopping their activity.

CONCLUSION

Study of Dronino iron ungrouped meteorite fragments in the clay sand was carried out using XRD and Mössbauer spectroscopy with a high velocity resolution. Surface oxidation products in two fragments found in the wet and drier clay sand appeared to be different. Ferric oxides and hydrous oxides were observed in the first fragment while in the second one siderite was additionally found. It was possible to distinguish the internal and external surface oxidation products in both fragments. In the fragment found in the wet clay sand the internal surface oxidation products contained ferric oxides and hydrous oxides while the external surface oxidation products consisted of ferric hydrous oxides. The weathering process of the second fragment found in drier clay sand showed the possible participation of bacteria which converted goethite into siderite observed in both internal and external surface oxidation products. The transfer of ferric hydrous oxides in the wet clay sand led to concretions formation from ferric hydrous oxides with different particles size.

Acknowledgment. This work was supported in part by the basic financing from the Ministry of Education and Science of Russian Federation (basic financing for the Projects # 2085 and # 1514) and by Act 211 Government of the Russian Federation, contract № 02.A03.21.0006.

REFERENCES

[1] V. I. Grokhovsky, M. I. Oshtrakh, O. B. Milder, V. A. Semionkin, *Bull. Russ. Acad. Sci., Phys.* **2005**, *69*, 1710.

[2] V. I. Grokhovsky, M. I. Oshtrakh, O. B. Milder, V. A. Semionkin, *Hyperfine Interact.* **2005**, *166*, 671.

[3] V. I. Grokhovsky, E. V. Zhiganova, M. Yu. Larionov, K. A. Uymina, M. I. Oshtrakh, *The Phys. Metals Metallogr.* **2008**, *105*, 177.

[4] M. I. Oshtrakh, V. I. Grokhovsky, E. V. Petrova, M. Yu. Larionov, K. A. Uymina, V. A. Semionkin, N. V. Abramova in *Proceedings of the International Conference "Mössbauer Spectroscopy in Materials Science 2008"* (Eds.: M. Mashlan, R. Zboril), AIP Conference Proceedings, Melville, New York **2008**, *1070*, 131.

[5] V. I. Grokhovsky, M. I. Oshtrakh, E. V. Petrova, M. Yu. Larionov, K. A. Uymina, V. A. Semionkin, *Eur. J. Mineral*. **2009**, *21*, 51.

[6] M. I. Oshtrakh, V. I. Grokhovsky, E. V. Petrova, M. Yu. Larionov, M. V. Goryunov, V. A. Semionkin, *J. Mol. Struct*. **2013**, *1044*, 268.

[7] M. I. Oshtrakh, A. A. Maksimova, M. V. Goryunov, G. A. Yakovlev, E. V. Petrova, M. Yu. Larionov, V. I. Grokhovsky, V. A. Semionkin, *Mössbauer spectroscopy with a high velocity resolution: advances in the study of meteoritic iron-bearing minerals* in *Proceedings of the Workshop on The Modern Analytical Methods Applied to Earth and Planetary Sciences* (Ed.: A. Gucsik), The MicroMatLab Kft Hungary, Sopron, **2015**, pp. 43–86.

[8] M. I. Oshtrakh, V. A. Semionkin, O. B. Milder, E. G. Novikov, *J. Radioanal. Nucl. Chem*. **2009**, *281*, 63.

[9] V. A. Semionkin, M. I. Oshtrakh, O. B. Milder, E. G. Novikov, *Bull. Rus. Acad. Sci.: Phys*. **2010**, *74*, 416.

[10] M. I. Oshtrakh, V. A. Semionkin, *Spectrochim. Acta, Part A* **2013**, *100*, 78.

[11] L. H. Bowen, S. B. Weed, *Mössbauer Spectroscopy of Soils and Sediments* in *Chemical Mössbauer Spectroscopy* (Ed.: R. L. Herber), Plenum Press, New York and London, **1984**, pp. 217–242.

[12] E. Murad, J. H. Johnston, *Iron Oxides and Oxyhydroxides* in *Mössbauer Spectroscopy Applied to Inorganic Chemistry*, Vol. 2 (Ed.: G. J. Long), Plenum Press, New York, **1987**, pp. 507–582.

[13] B. A. Goodman, *Mössbauer Spectroscopy* in *Clay Mineralogy: Spectroscopic and Chemical Determinative Methods* (Ed.: M. J. Wilson), Chapman & Hall, London, **1994**, pp. 68–119.

[14] R. Zboril, M. Mashlan, D. Petridis, *Chem. Mater*. **2002**, *14*, 969.

[15] E. Murad, J. Cashion, *Mössbauer Spectroscopy of Environmental Materials and their Industrial Utilization*, Kluwer Academic Publishers, New York, **2004**, p. 418.

[16] E. Murad, *Clay Miner*. **2010**, *45*, 413.

[17] M. I. Oshtrakh, M. V. Ushakov, B. Senthilkumar, R. Kalai Selvan, C. Sanjeeviraja, V. A. Semionkin, *Proceedings of the International Conference "Mössbauer Spectroscopy in Materials Science 2012"* (Eds.: J. Tuček, L. Machala), AIP Conference Proceedings, Melville, New York, **2012**, *1489*, 115.

[18] M. I. Oshtrakh, M. V. Ushakov, B. Senthilkumar, R. Kalai Selvan, C. Sanjeeviraja, I. Felner, V. A. Semionkin, *Hyperfine Interact*. **2013**, *219*, 7.

[19] I. Mitov, D. Paneva, B. Kunev, *Thermochim. Acta* **2002**, *386*, 179.

[20] S. Musić, S. Popović, *J. Radioanal. Nucl. Chem.* **1987**, *111*, 27.

[21] B. B. Ellwood, B. Burkart, K. Rajeshwar, R. L. Darwin, R. A. Neeley, A. McCall, G. J. Long, M. L. Buhl, C. W. Hickcox, *J. Geophys. Res.* **1989**, *94*, 7321.

[22] S. Ram, K. R. Patel, S. K. Sharma, R. P. Tripathi, *Fuel* **1998**, *77*, 1507.

[23] G. Medina, J. A. Tabares, G. A. Pérez Alcazar, J. M. Barraza, *Fuel* **2006**, *85*, 871.

[24] B. Maitte, F. P. A. Jorand, D. Grgic, M. Abdelmoula, C. Carteret, *Chem. Geol*. **2015**, *412*, 48.